This is a repository copy of *The Superstatistical Nature and Interoccurrence Time of Atmospheric Mercury Concentration Fluctuations*.

The Superstatistical Nature and Interoccurrence Time of Atmospheric Mercury Concentration Fluctuations

Correspondence to:
F. Carbone,
f.carbone@iia.cnr.it

F. Carbone[1], A. G. Bruno[1,2], A. Naccarato[1], F. De Simone[1], C. N. Gencarelli[1], F. Sprovieri[1], I. M. Hedgecock[1], M. S. Landis[3], H. Skov[4], K. A. Pfaffhuber[5], K. A. Read[6], L. Martin[7], H. Angot[8,9], A. Dommergue[8], O. Magand[8], and N. Pirrone[10]

[1]CNR-Institute of Atmospheric Pollution Research, Division of Rende, UNICAL-Polifunzionale, Rende, Italy, [2]Dipartimento di Fisica, Università della Calabria, Rende, Italy, [3]U. S. Environmental Protection Agency, Office of Research and Development, Research Triangle Park, Durham, NC, USA, [4]Department of Environmental Science, Aarhus University, Roskilde, Denmark, [5]Norwegian Institute for Air Research (NILU), Kjeller, Norway, [6]NCAS, National Centre for Atmospheric Sciences, University of York, York, UK, [7]Cape Point GAW Station, Climate and Environment Research and Monitoring, South African Weather Service, Stellenbosch, South Africa, [8]University Grenoble Alpes, CNRS, IRD, IGE, Grenoble, France, [9]Now at Institute for Data, Systems, and Society, Massachusetts Institute of Technology, Cambridge, MA, USA, [10]CNR-Institute of Atmospheric Pollution Research, Area della Ricerca di Roma 1, Monterotondo, Italy

Abstract The probability density function (PDF) of the time intervals between subsequent extreme events in atmospheric Hg^0 concentration data series from different latitudes has been investigated. The Hg^0 dynamic possesses a long-term memory autocorrelation function. Above a fixed threshold Q in the data, the PDFs of the interoccurrence time of the Hg^0 data are well described by a Tsallis q-exponential function. This PDF behavior has been explained in the framework of superstatistics, where the competition between multiple mesoscopic processes affects the macroscopic dynamics. An extensive parameter μ, encompassing all possible fluctuations related to mesoscopic phenomena, has been identified. It follows a χ^2 distribution, indicative of the superstatistical nature of the overall process. Shuffling the data series destroys the long-term memory, the distributions become independent of Q, and the PDFs collapse on to the same exponential distribution. The possible central role of atmospheric turbulence on extreme events in the Hg^0 data is highlighted.

1. Introduction

A number of studies using different methodologies have shown that long-term memory in atmospheric pollutant concentrations exists (Chelani, 2016; Lovejoy & Schertzer, 2013; Tuck, 2010), that is, up to a limit the concentrations maintain a certain correlation over time. Usually a long-term memory process is defined by a strong coupling between measured values at different time lags, ℓ, and the system's dynamics are characterized by the presence of complex mesoscopic spatiotemporal patterns. These patterns are associated with the generation of high-amplitude fluctuations over a broad range of spatial and temporal scales giving rise to scale-free relationships for statistical quantities (Frisch, 1995; McComb, 1990; Monin & Yaglom, 2007). These mesoscopic processes occur within macroscopic phenomena, and their behavior evolves into a power law decay of the autocorrelation function. Conversely, in a short-term memory process the autocorrelation function decreases exponentially or to zero after a certain time, ℓ. The dynamics of pollutant concentration variations depend on numerous processes, (for a review see Chelani, 2016); however, due to their complexity it is not possible to precisely describe their behavior and properties over space and time. One of the principal characteristics of complex dynamical systems is the intermittency (Briggs & Beck, 2007; Carbone & Sorriso-Valvo, 2014; Carbone, Gencarelli, et al., 2016; Manshour et al., 2016; Warhaft, 2000). Intermittency represents the strongly correlated fluctuations that lead to deviations from a normal probability distribution function (PDF). In the atmospheric boundary layer, intermittency is an important part of a continuous spectrum of atmospheric motions (Katul et al., 2006; Vindel & Yagüe, 2011; Wyngaard, 1992). Within large-scale temporal variations of atmospheric motion, fluctuations in pollutant species concentrations result from interactions of a large ensemble of mesoscopic phenomena, occurring contemporaneously in the atmosphere: turbulence (Wyngaard, 1992), variation in anthropogenic and natural emission sources (Carbone, Landis, et al., 2016;

Pirrone et al., 2010), variation in deposition velocity, loss through chemical reactions that is in turn determined by fluctuating reactant/oxidant concentrations, and other extreme events. In the specific case of Hg^0 these extreme events would include phenomena such as convective storms, forest fires, and atmospheric Hg^0 depletion events (De Simone et al., 2017; Dvonch et al., 2005; Holmes et al., 2016; Lindberg et al., 2002; Schroeder et al., 1998). Understanding the dynamics of these emergent extreme events, meteorological, chemical, and anthropological, represents the key to understanding complex dynamical systems.

Due to their complexity, the analysis of these systems has focused on the understanding of where certain features are exhibited by a large class of phenomena, regardless of the details of their structure (Manshour et al., 2016). Beck and Cohen (2003) have shown that complex nonequilibrium systems, which possess a spatiotemporally fluctuating intensive quantity, can often be effectively described by a superposition of statistics, so-called "superstatistics." The core idea is to characterize the system under consideration as a superposition of several statistics, which act on different time scales (Beck et al., 2005; Beck, 2010). Importantly for this study, it has been shown that a suitable intensive parameter μ of the complex system, (e.g., a local variance parameter extracted from an experimental data set) exists, which generates a Tsallis q-distribution if μ is a χ^2-distributed random variable (Abe & Okamoto, 2001; Briggs & Beck, 2007; Manshour et al., 2016; Tsallis, 1988; Tsallis et al., 1998). Therefore, an understanding of sudden (intermittent) atmospheric events could provide useful information about climatological phenomena, teleconnections, and atmospheric transport processes (Bunde et al., 2005). Although the atmosphere is a relatively minor reservoir of Hg^0 compared to other environmental compartments, it is an important pathway by which Hg^0 is distributed globally over relatively short timescales, once thought to be roughly a year, but more recently closer to 6 months (Horowitz et al., 2017; Schroeder & Munthe, 1998). Efforts to measure Hg concentrations in monitoring networks worldwide and interpret these data with models have increased recently, seeking to elucidate the way Hg cycles in the environment (Pirrone et al., 2010). A number of important issues remain unexplained due to the complex interactions of Hg species, with and within, a multiphase atmospheric matrix that is in a constant state of flux. The focus here is on the long-term memory of atmospheric Hg^0 concentrations observed at different latitudes and their sudden or extreme (intermittent) events through analysis of the interoccurrence times (IOTs) of Hg^0 concentration fluctuations. The superstatistical nature of these extreme events has been investigated and demonstrated.

1.1. Hg^0 Measurements Methods

The atmospheric Hg^0 data used in this analysis were all obtained using automated Tekran (Toronto, Canada) Model 2537A cold vapor atomic fluorescence spectrometer instruments. Tekran equipment provides a detection limit below 0.1 ng/m^3 and a linear response over the range 1–200 ng/m^3 within 2%. The instruments are calibrated periodically using the internal permeation source in accordance with the Global Mercury Observation System (GMOS) standard operating procedure (every 72 h with a permeation time of 120 s). Details of the instrument operating parameters can be found in Carbone, Landis, et al. (2016), Landis et al. (2002), Sprovieri et al. (2016), and Steffen et al. (2015). An exhaustive description of most of the sampling sites including their location, altitude, and climatology, as well as the Hg^0 data quality assurance/quality control (QA/QC) protocols, for data quality assessment, can be found in Sprovieri et al. (2016). The original data set had a temporal resolution of $\Delta t = 300$ s; however, some data were excluded by the QA/QC procedure employed in order to ensure data quality. There, the temporal resolution was reduced to $\Delta t = 3,600$ s; this allowed a good compromise between the sample length and data set sampling at different thresholds, Q.

2. Superstatistics and Interoccurrence Times

Superstatistics seeks to represent a complex nonequilibrium system as a superposition of two (or several) statistics, described by an intensive parameter μ that fluctuates on a relatively large spatiotemporal scale (Beck & Cohen, 2003; Briggs & Beck, 2007). Thus, μ might itself be a stochastic variable that incorporates all the possible fluctuations (a local emergent dynamic or competition in the mesoscopic subparts of the system), which produces a sudden variation in the collective dynamic (Beck, 2010). If μ is distributed according to a probability density $f(\mu)$, then the long-term associated marginal probability of the physical process $P(\tau)$ (τ being the time lag between two subsequent events) may then defined as a mixture of exponential distributions within which μ fluctuates (Beck, 2010; Manshour et al., 2016; Tsallis & Souza, 2003):

$$P(\tau) = \int_0^\infty \mu f(\mu) e^{-\mu \tau} d\mu \qquad (1)$$

As defined by Beck and Cohen (2003), $f(\mu)$ cannot be a generic function but must be a normalized probability density, a physically relevant density from statistics (for instance, Gaussian, uniform, chi-squared, log normal but potentially others also), and must be normalizable (the integral $\int_0^\infty P(\tau)d\tau$ must exist). The superstatistical parameter μ does not necessarily have to be a variable such as inverse temperature, but it could be an effective parameter in a stochastic differential equation, a volatility measure in finance or simply a local variance parameter extracted from an experimental time series, as in the case described here (Beck, 2010). In this last case, μ can be extracted from an experimental data series by partitioning the original data set in M nonoverlapping windows of fixed size and taking the inverse variance of the data contained within each window (Kosun & Ozdemir, 2016; Rabassa & Beck, 2015).

When a process is random or uncorrelated, the PDF collapses on to an exponential distribution, and in general, the zeroth-order theoretical model for the distribution $P(\tau)$ can be written as $P(\tau) = \mu e^{-\mu\tau}$ (Briggs & Beck, 2007; Manshour et al., 2016; van Kampen, 1981). In that case, equation (1) reduces to the exponential model if there are no fluctuations of the intensive parameter μ, and the distribution $f(\mu)$ is a delta function. Any deviation of $f(\mu)$ from a delta function yields a nonexponential $P(\tau)$.

If $f(\mu)$ follows a χ^2 distribution (equation (2))

$$f(\mu) \sim \mu^{k/2-1} \exp\left[-\frac{k\mu}{2\mu_0}\right],$$

(2)

with k degrees of freedom (μ_0 is a constant), the corresponding superstatistics, obtained by integrating over all μ, is described by a q statistic (Abe & Okamoto, 2001; Tsallis, 1988; Tsallis et al., 1998).

Hence, the behavior of the PDF is described by a Tsallis q-exponential function (equation (3)) and possesses asymptotic power laws (Briggs & Beck, 2007; Manshour et al., 2016):

$$P(\tau) = \frac{\alpha}{[1 + \beta(q-1)\tau]^{1/(q-1)}},$$

(3)

where α is a normalization factor (Beck, 2010; Wilk & Włodarczyk, 2000), q is a measure of the deviation from an exponential distribution, and $q > 1$ indicates a long-tailed distribution. A number of authors have shown that the limit of validity for the parameter q lies in the range $1 \leq q \leq 2$. The upper limit arises from the normalization condition of $P(\tau)$ to the unit area and the requirement that the normalization constant, α, is positive (Briggs & Beck, 2007; Douglas et al., 2006; Tsallis, 1988; Wilk & Włodarczyk, 2000). The behavior of the q exponential is principally related to a long-term memory process and also to the presence of strong ramp-cliff or extreme events in the data. The atmosphere is a complex system, described by a large number of variables, which are nonlinearly coupled by competing physical and chemical processes. The competition among processes becomes evident once the observations of a single variable are dominated by sudden and intermittent fluctuations. Variables can be either active or passive, transported by the atmospheric flow, or feeding back (and thus modifying) the flow itself (Celani et al., 2004; Mazzitelli & Lanotte, 2012).

This study focuses on fluctuations in Hg^0 concentration, which is hypothesized to be governed by a combination of large-scale atmospheric flow and mesoscopic (small-scale) processes. The aim is to investigate whether the statistics of the Hg^0 data series can provide insights into the similarities or differences between the measurement sites. Such an investigation requires that the data set is suitable for the proposed analysis. Rabassa and Beck (2015) lay out a series of criteria that may be used in this context. These criteria concern the skewness and kurtosis of the data set, the existence of an appropriate time scale separation, and the reasonableness of a local Gaussian approximation. Applying the strategy proposed in Van der Straeten and Beck (2009), the short time scale t_S has been found to be between $t_S \in [6 \div 11]$ h, while the long time scale found is $t_L > 50$ h. The ratio of $t_S/t_L \approx 0.2$ is comparable with the case presented in Rabassa and Beck (2015). As a further check on the assumption that during long-range transport, Hg^0 concentration may be considered a real passive scalar quantity, and the Hurst exponent can be evaluated. This can then be compared to the value of $H = 5/9$ predicted by generalized scale invariance, see Tuck (2010). The average Hurst exponent extracted from the data series used here is in good agreement with the value $H = 5/9$ (Istas & Lang, 1997; Tuck, 2010): Troll (TRL 72°S, 2°E) $H = 0.58 \pm 0.02$, Mauna Loa, Hawaii (MLO 19°N, 155°W) $H = 0.49 \pm 0.10$, and Ny Alesund (NYA 78°N, 11°E) $H = 0.53 \pm 0.01$.

Three sample Hg^0 concentration data sets are shown in Figure 1, for Villum Research Station at Station Nord, Greenland (81°N, 17°W), Mauna Loa, Hawaii, and Troll, Antarctica.
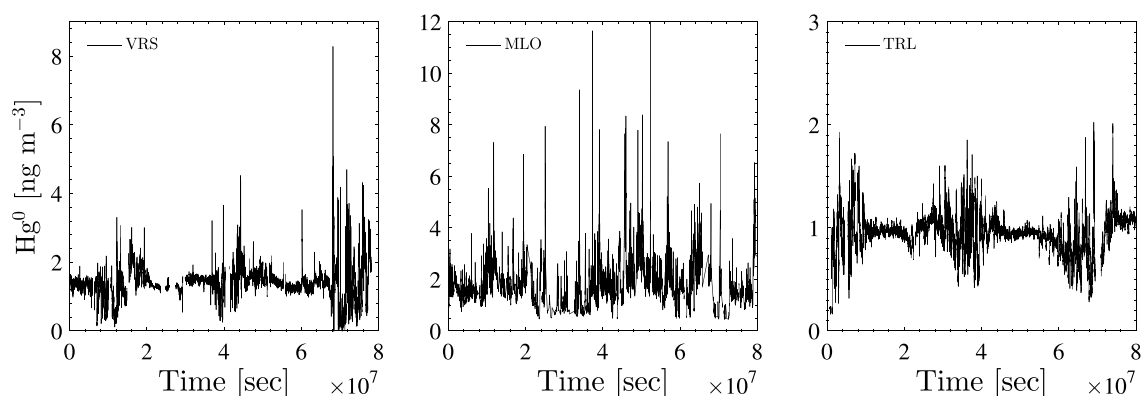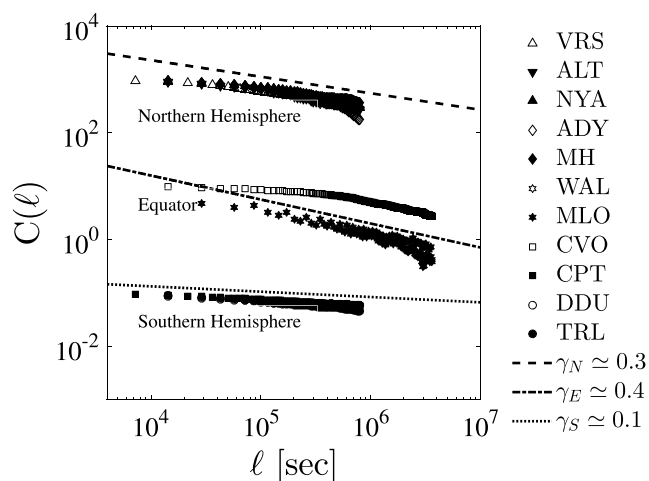
Figure 1. Hg^0 data measured at three different sites: (left) Villum Research Station at Station Nord (VRS 81°N, 17°W), (middle) Mauna Loa Observatory (MLO 19°N, 155°W), and (right) Troll (TRL 72°S, 2°E).

The intermittent nature of the Hg^0 data is characterized by alternating periods of strong fluctuations and smoother periods characterized by smaller fluctuations. This behavior is determined by a large ensemble of mesoscopic phenomena occurring in the atmosphere. Despite this intermittent dynamic, the phenomenon preserves its non-Markovian nature, since a power law decay in the autocorrelation function is observed (Figure 2) (Alder & Wainwright, 1970; Bunde et al., 2005; Chelani, 2016; Schertzer & Lovejoy, 1985, 1987). If $x(t)$ represents the instantaneous concentration of Hg^0 at time t, the associated autocorrelation function may be written as

$$C(\ell) = \frac{1}{\sigma_x^2(T-\ell)} \sum_{t=1}^{T-\ell}(x(t) - \langle x \rangle)(x(t+\ell) - \langle x \rangle) \sim \ell^{-\gamma}, \tag{4}$$

where ℓ represents the time lag, and σ_x is the standard deviation of $x(t)$. Due to the passive scalar nature of Hg^0, the standard deviation of the concentration is related to atmospheric eddy diffusivity and represents a measure of the characteristic width of the plume (Hayley et al., 2002).
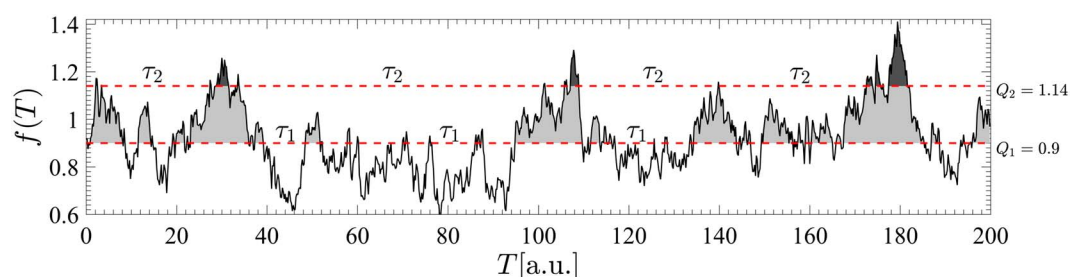
All the stations in a given hemisphere present the same scaling, and those close to the equator (tropics) present a scaling faster than those at higher latitudes, $\gamma_E \approx 0.4$, $\gamma_N \approx 0.3$, and $\gamma_S \approx 0.1$, respectively, for tropics, Northern Hemisphere, and Southern Hemisphere. It appears that $C(\ell)$ within either of the three zones is independent of latitude. A slight difference occurs in the tropical stations, the Cape Verde Observatory (CVO) and MLO, at small scale (small ℓ). At larger scales (longer ℓ) the scaling is in perfect agreement for both stations $\gamma_E \approx 0.4$. The curves $C(\ell)$ in Figure 2 have been vertically shifted for clarity.

The presence of long-range correlations suggest that there might be some other fundamental process (or processes) embedded in the temporal evolution of the Hg^0 data series, as seen with other pollutants (Chelani, 2016).

The greater the irregularity of the mesoscale processes occurring in the atmosphere the faster the system "loses its memory." In this case these processes would include sources, sinks such as dry deposition or wet scavenging, and chemical transformations. One possible hypothesis to explain the differences in the slopes in the three latitude zones may be the different characteristics of Hg0 emissions in each. Hg0 emission in the tropics includes biomass burning that is irregular, another factor may be the different characteristics of Hg^0 emissions in each. Hg^0 emission in the tropics includes biomass burning that is irregular, another factor may be that meteorological phenomena also tend to be of shorter duration (De Simone et al., 2015). The Northern Hemisphere is the home to most of the world's anthropogenic emission sources and also has biomass burning events. The Southern Hemisphere in comparison has less variable and lower Hg^0 emissions, and synoptic rather than local weather conditions often dominate in large regions.

Figure 2. Power law decay of Hg^0 data with slopes $\gamma_N = 0.3$, $\gamma_E = 0.4$, and $\gamma_S = 0.1$, respectively for the Northern Hemisphere, tropics, and Southern Hemisphere. The curves have been vertically shifted for clarity.

Figure 3. Sample illustration of IOT, τ_i, obtained from a synthetic data set. Horizontal dashed lines represent the selected threshold Q in the data. By increasing Q, two sets of IOT $\tau_{1,2}$ can be identified in the data, characterized by an increasing average $\langle \tau_i \rangle$ and standard deviation σ_τ, respectively.

An optimal method used to obtain information concerning extreme events in physical or chemical processes is IOT, τ, series analysis. IOTs are a measure of the time between the occurrence of two or more subsequent events in the data that exceed a fixed, threshold Q_i (Figure 3). The events exceeding Q are defined as rare or more usually extreme. If a long-range correlation exists in the data, then the IOTs, τ_i, are also long-range correlated (Bogachev & Bunde, 2008; Bogachev et al., 2007; Eichner et al., 2007; Ferri et al., 2010, 2012; Santhanam & Kantz, 2005).

Before performing the IOT analysis, the standard normalization procedure, (subtracting the mean value of the data and dividing by the standard deviation) was applied to the Hg^0 data. Following this strategy, performing the analysis at a generic threshold Q implies performing the analysis at a fixed standard deviation value of the data. This procedure is required in order to facilitate the comparison of concentration data measured at different latitudes. For every Q, an average $\langle \tau \rangle$ and standard deviation σ_τ are defined, and by increasing Q, $\langle \tau \rangle$ and σ_τ become larger. The higher the Q, the rarer or more extreme are the events. Also, there is a one-to-one correspondence between Q and the $\langle \tau \rangle$, σ_τ values (Figure 4, middle and right columns) (Chelani, 2016). The differences between the three normalized data sets are shown in Figure 4, second row. At MLO the
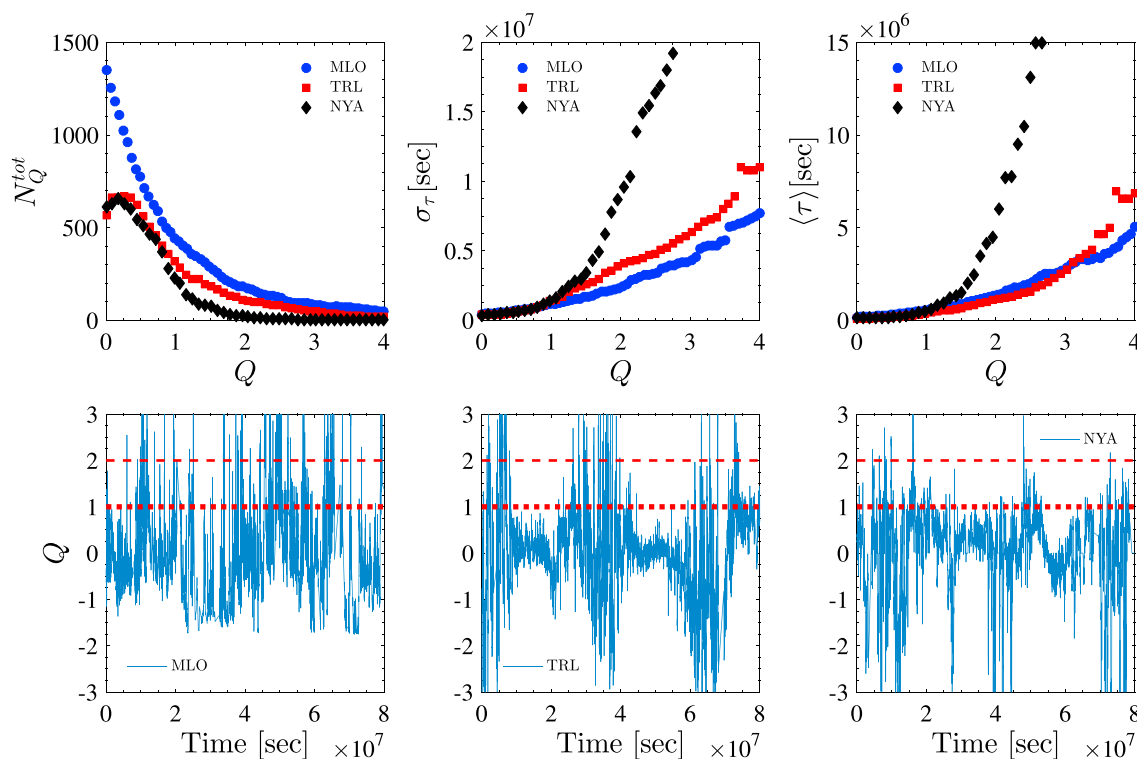
Figure 4. (first row) Dependence on the threshold Q of the parameters N_Q^{tot}, σ_τ, and the average $\langle \tau \rangle$ of the IOT, measured at three very different latitudes: Mauna Loa (MLO 19°N, 155°W), Troll (TRL, 72°S, 2°E), and Ny Alesund (NYA 78°N, 11°E). (second row) Comparison of the three normalized data set.

dynamic is characterized by a large number of spikes where $Q > 0$, which can be related to volcanic (Landis et al., 2013), oceanic (Carbone, Landis, et al., 2016), Hg^0 emissions or to long-range atmospheric transport phenomena. TRL and NYA data show a very different dynamic, characterized by strong fluctuations at both positive and negative Q. The negative fluctuation is related to Hg depletion events (Steffen et al., 2008). However, in the range $Q \in [0 \div 1.5]$ the data set from each site demonstrates the same behavior, characterized by a wide distribution of IOT with the same $\langle \tau \rangle$ and σ_τ (Figure 4, first row). The strong departure of the value of σ_τ and $\langle \tau \rangle$ for the NYA data set is related to the lower number of positive ($Q > 0$) fluctuations (Figure 4, bottom right). In this case, by increasing the threshold $Q > 1$ (dotted line in Figure 4, second row) the IOT duration becomes longer, but at the same time the number of IOT N_Q^{tot} decreases due to the distance between two subsequent peaks, resulting in a rapid increase in σ_τ.

Investigating a real passive scalar such as Hg^0 is also interesting from a fundamental point of view, because its dynamics are mainly, if not completely, related to turbulent eddies in the atmosphere.

3. Discussion

The PDFs of the IOT, $P(\tau)$, from the normalized Hg^0 data were evaluated by using a number of bins, N_{bins} ($N_{bins} \in [10 \div 15]$), depending on the specific data set; this choice being principally due to the temporal resolution of the data ($\Delta t = 3,600$ s). For every threshold Q, the range of the PDF bins was set between the minimum and maximum values of τ in logarithmically spaced bins of length A_{bins}. However, as it is the PDFs that are calculated, the number of bins and their width are irrelevant to the analysis. The histogram of the IOT, $N_Q(\tau)$, has been used to calculate the PDF $P(\tau) = N_Q(\tau)/(A_{bins} N_Q^{tot})$, where c is the total number of observations (IOT) at a fixed threshold Q (Figure 4, top left). Figure 4 shows the standard deviation σ_τ and the average $\langle \tau \rangle$ of the IOT for three very different latitudes. All the experimental data sets demonstrate universal scaling for these two quantities over the range $Q \in [0 \div 1.5]$. For this reason all the following analyses were performed using this range of Q.

The sampling uncertainty on each bin of $P(\tau)$ is calculated from the statistical (Poisson) error on the histogram $Err[N(x)] = \sqrt{N(x)}$, which, following the error on the probability density, becomes $Err[P(\tau)] = \sqrt{P(\tau)/(A_{bins} N_Q^{tot})}$. Outside a given range, roughly $Q \geq 2.5 \div 3$ (related to the size of the Hg^0 data set), the statistics are too poor to permit accurate analysis, since the relative statistical error becomes too large.

Due to the strong fluctuations a threshold $Q > 0.5$ (site dependent) is sufficient to observe an interesting dynamic. At this value a large number of IOTs can be identified, characterized by $\sigma_\tau = 15 \pm 1$ days (Figure 6). Figure 6 shows the PDFs, for three different sites, of the Hg^0 IOT extremes (log-log plot). The plots have been shifted vertically for clarity. It is worth noting that for each Q, the values of τ can be drastically different. Rather than $P(\tau)$, in order to compare the different distributions of the IOT, the PDF of the normalized IOT $P(\tau/\sigma_\tau)$ was evaluated. This procedure ensures that for every Q the values of τ/σ_τ always lie in the same interval. To check the universality of the q exponential, the analysis has been performed at different values of Q for each normalized data set. Figure 5 shows the PDF $P(\tau/\sigma_\tau)$ (symbols), obtained for different sites at various thresholds Q. The same figure also shows the relative q exponential fit obtained from equation (3). The fitting procedure was performed by minimizing the χ^2 statistic by varying the model parameters (equation (3)): q within the closed interval $q \in [1 \div 2]$, while the other parameters in the open interval $\alpha, \beta \in (0 \div \infty)$. As stated in section 1.1, uncertainties should be minimized to obtain an accurate estimate of $P(\tau)$. A large number of gaps in the data set could potentially mask the real distribution. Long gaps give raise to a fat-tailed PDF, because the length of a certain number of IOTs can be overestimated, and the exponent q in equation 3 can exceed the theoretical value $q > 2$. In case of multiple short gaps, especially for $Q \approx 0$, the exponent q tends to unity. In this case the theoretical distribution, equation (3), is characterized by a fast decay, and the fitting procedure is unable to fully capture the tail of the PDF.

The value of τ ranges from 1.21×10^4 s to 2.42×10^7 s (approximately 3 h to 9 months, the latter being roughly compatible with the average residence time of Hg^0 in the atmosphere), which in terms of τ/σ_τ is translated into an interval $\tau/\sigma_\tau \in [10^{-2} \div 10^1]$. The values of σ_τ, used for the normalization, are shown in Figure 6. The behavior of the PDFs illustrates the good agreement between the q exponential (equation (3)) and the data over the whole range of normalized IOTs $\tau/\sigma_\tau \in [10^{-2} \div 10^1]$ (Figure 5). The value of q exponential reported in Figure 5 represent the average obtained over the different thresholds Q reported in the figure.
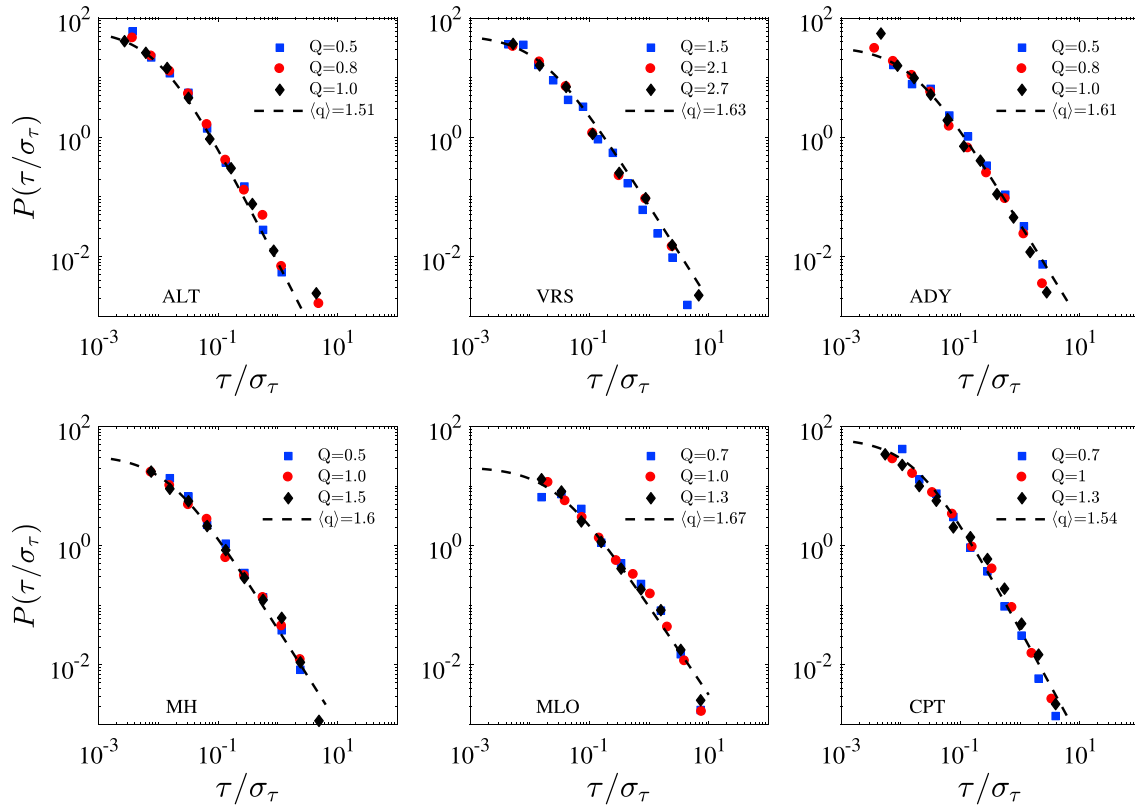
Figure 5. Log-log plot of PDF $P(\tau/\sigma_\tau)$ for the normalized IOT extracted from Hg^0 data recorded at different latitudes and different threshold Q. Dashed line is the averaged q exponential fit (equation (3)).
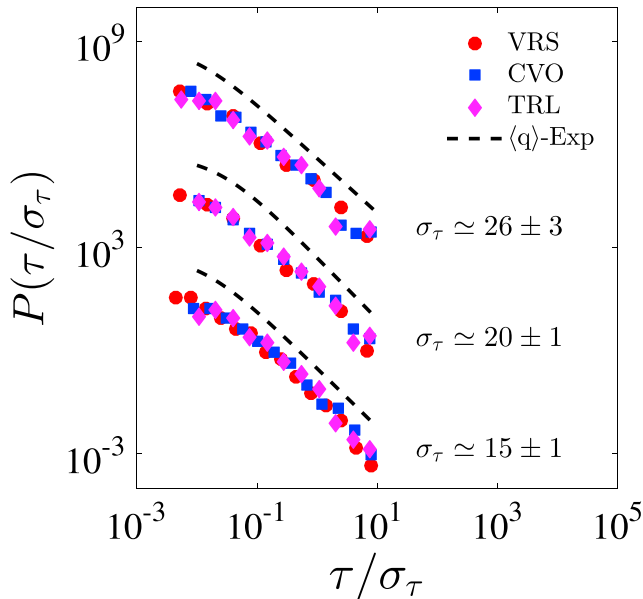

Figure 6. Log-log plot of PDFs $P(\tau/\sigma_\tau)$ for the normalized IOT obtained at three different sites and at three different thresholds Q: VRS 81°N, 17°W), CVO, and TRL 72°S, 2°E). The plots have been arbitrarily shifted vertically for clarity. For VRS, $Q=0.6, 1.3, 1.5$; CVO, $Q=0.7, 0.9, 1$; and TRL, $Q=0.9, 1.1, 1.3$. For these thresholds all the data possess the same σ_τ. Dashed lines are the q exponential fit (equation (3)).

From Figure 5 it is evident that the normalization process is robust since no difference can be observed in the distribution $P(\tau/\sigma_\tau)$ when varying the threshold Q.

In Figure 6 the PDFs $P(\tau/\sigma_\tau)$ have been grouped according to the value of σ_τ: $\sigma_\tau = 15 \pm 1$, $\sigma_\tau = 20 \pm 1$, and $\sigma_\tau = 26 \pm 3$ days, respectively. In this way it may easily be observed that for three very different latitudes: VRS (Arctic), CVO (Tropics), and TRL (Antarctica) all the PDFs converges on the same universal q-exponential distribution 3. The curves have been vertically shifted for clarity.

The normalization factor α (equation (3)) reflects the value $\alpha_{th} = \beta(2 - q)$ as found in Manshour et al. (2016): for MLO at $Q=1$ the values obtained from the q–exponential fit for $\alpha = 18.7 \pm 1$, $q = 1.55 \pm 0.1$, and $\beta = 40 \pm 3$, using the relation above, give $\alpha_{th} = 18 \pm 3$. The same result is obtained for the other stations: VRS $Q = 1.2$, $\alpha = 47 \pm 1$, $q = 1.53 \pm 0.07$, $\beta = 81 \pm 6$, and $\alpha_{th} = 38.1 \pm 6.1$; CVO $Q=1.2$, $\alpha = 17 \pm 2$, $q = 1.54 \pm 0.12$, and $\beta = 37 \pm 7$, and $\alpha_{th} = 17.02 \pm 7$. Similar agreement was found for all the other stations. These results assure the goodness of the q statistics in describing extreme events in the Hg^0 time series at different latitudes. The PDFs clearly display the same behavior and could be represented by the universal law, equation (3), with the same q parameter. The values of q obtained over all latitudes lie in the range $q \in [1.3 \div 1.7]$ and are distributed around an average value $\langle q \rangle \approx 1.59 \pm 0.05$ (Figure 7). This result makes evident the universality of the mechanism that lies behind the IOTs within the Hg^0 concentration time series. The results shown in Figure 2, on the other hand, demonstrate the variation with latitude of the local, that is mesoscale, phenomena. Figure 7 shows that the formation of IOTs is a
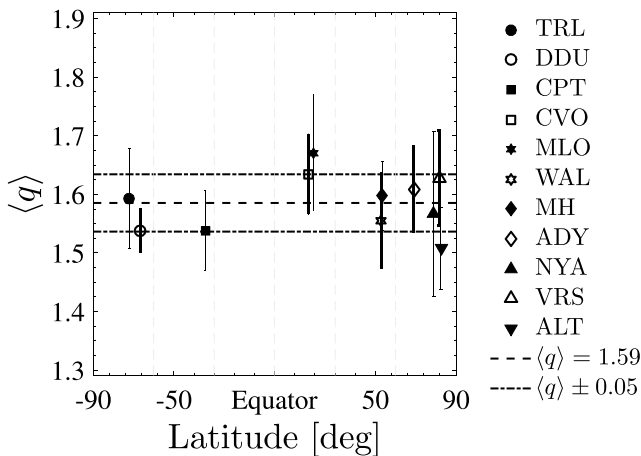
Figure 7. Average $\langle q \rangle$ ent Q thresholds. All values are distributed around the dashed line $\langle q \rangle = 1.59 \pm 0.05$. Dash-dotted lines represent the standard deviation of the experimental q values. Hg^0 data from the following sites were included: TRL 72°S, 2°E), Dumont d'Urville (DDU 66°S, 140°E), Cape Point (CPT) 34°S, 18°E), CVO 16°N, 24°W), Mace Head (MH 53°N, 9°W), Waldhorf (WAL 52°N, 10°E), Ny Alesund (NYA 78°N, 11°E), Andoya (ADY 69°N, 16°E), VRS (81°N, 17°W), and Alert (ALT 82°N, 62°W).

large-scale characteristic of the time series, and that it is universal and independent of latitude.

This q value is significant since a similar value has been reported in a different context, namely velocity fluctuations in fully developed turbulence experiments (Manshour et al., 2016), where $q \approx 1.6$ was obtained from the IOT statistics. In light of this, it becomes clear that atmospheric turbulence, although it is never fully developed in the atmosphere, potentially plays a central role in the Hg^0 IOT dynamic.

For comparison Figure 8 shows the PDFs of the normalized IOT τ^W, obtained from 1 min (top row) and 1 h (bottom row), wind velocity data recorded at Mauna Loa Observatory. The analysis was performed on two different data sets sampled during the years 2015 and 2016, while a third data set covers the period 2012–2016. In these cases the q values obtained are in perfect agreement with the results from laboratory experiments (Manshour et al., 2016), demonstrating the universality of the phenomenon. The q values found were $q = 1.58$, 1.59 and 1.61 for the 2015, 2016, and 2012–2016 1 min data sets, and $q = 1.6$, 1.55 and 1.6 for the 1 h data sets. It should be pointed out that the full data series were used and not selected to use only daytime or nighttime data even though the wind regimes change significantly between day and night on MLO, see Ryan (1997) and Sharma and Barnes (2016).

In light of this result, it becomes evident that the variation from $q \approx 1.6$ could be related to other factors that influence the dynamics. For example, at MLO $\langle q \rangle = 1.67$, however, volcanic emissions near MLO are known to emit Hg^0 and may act as a local perturbation to the large-scale dynamics. Continuous perturbations of this nature could shift the exponent q away from the dominant dynamic, where the exponent should be $q \approx 1.6$.
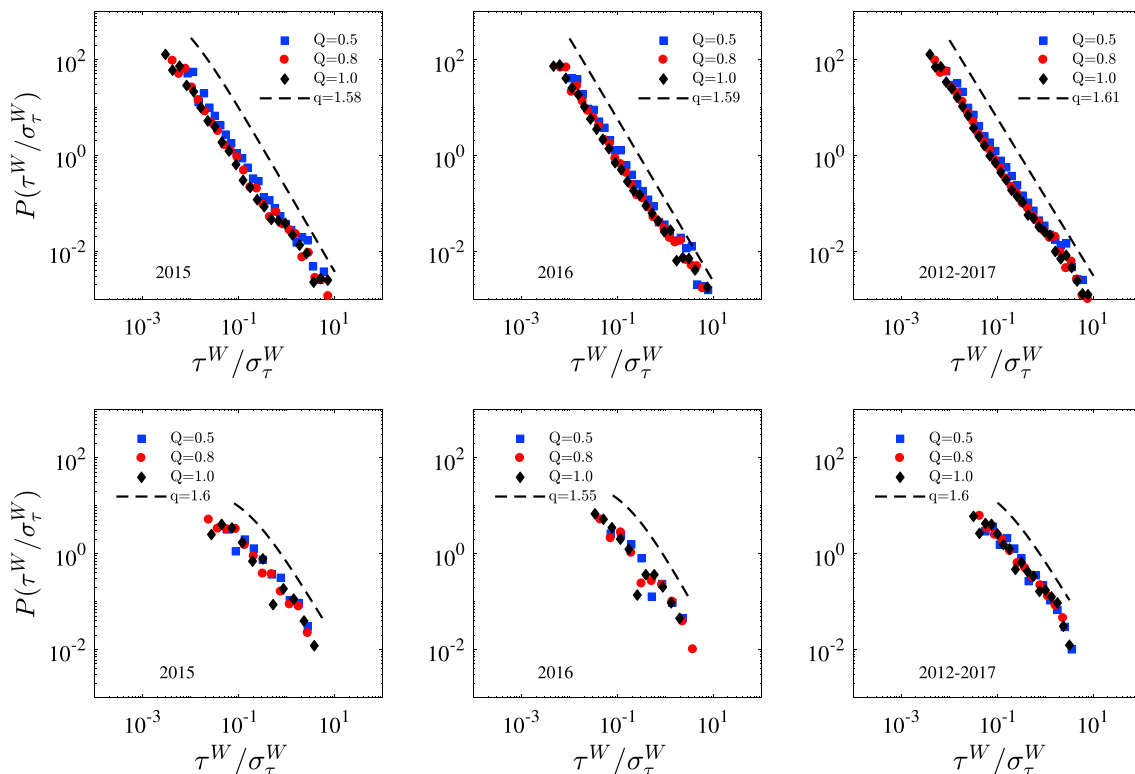
Figure 8. (top row) A log-log plot of PDFs $P(\tau^W/\sigma_\tau^W)$ for the normalized IOT evaluated from 1 min wind speed data at MLO, for three different data sets. (bottom row) Log-log plot of PDFs relative to the 1 h wind speed data, the same data sets has been used. Dashed line is q-exponential fit 3.
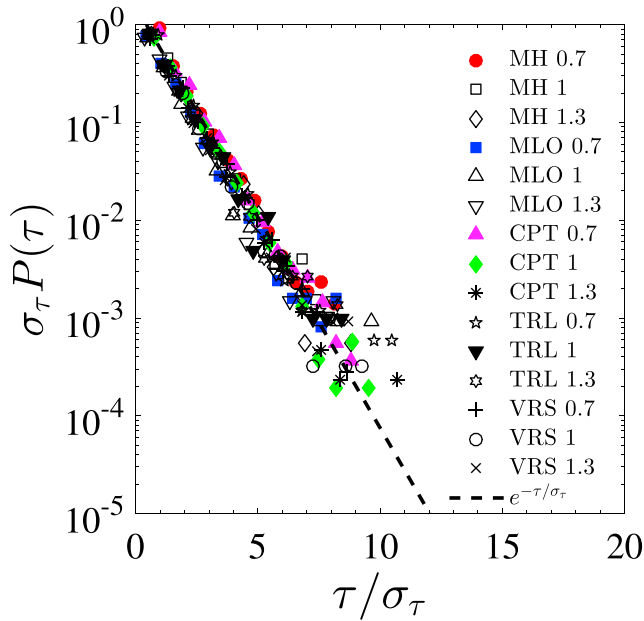
Figure 9. Log linear plot of PDFs $P(\tau/\sigma_\tau)$, for four stations, after the random permutation of the original data. The PDFs are independent of the threshold Q and collapse on the same exponential distribution, exposing their uncorrelated nature. Numbers next to the station label in legend represent the Q value. The stations reported in the plot are Mace Head (MH 53°N, 9°W), MLO, Cape Point (CPT 34°S, 18°E), TRL, and VRS. All the other stations show the same behavior but have not been included for figure clarity.

In the case of a nonexponentially decaying PDF, the shape indicates the presence of correlated structures in the process (long-term memory in the phenomenon) (Bogachev & Bunde, 2008; Bogachev et al., 2007; Chelani, 2016; Eichner et al., 2007; Ferri et al., 2010, 2012). To check the dependence of the correlated structure in the data set, the Hg^0 data were randomly rearranged over a large number of trials, keeping the random seed fixed. Figure 9 shows the PDF of the shuffled data set in a log linear plot. The random permutation destroys the correlation in the data, and moreover, the distribution becomes independent of the threshold Q and collapses onto the same exponential shape: $P(\tau) = \sigma_\tau^{-1} \exp^{-\tau/\sigma_\tau}$.

In this framework a single measurement can be related to a local emergent dynamic in the system or can encompass all the possible mechanisms capable of producing a sudden variation in the collective dynamic of the system. Recalling equation (1), $\mu = \sigma_\tau^{-1}$ is the parameter that incorporates all the possible fluctuations due to competing processes in the mesoscopic dynamics of the system. Since most IOTs are very sharp for large values of $\mu(\sigma_\tau)$, whereas small values of μ correspond to the frequent occurrence of long IOTs, the existence of correlations in the dynamics makes μ a fluctuating random variable with a probability density $f(\mu)$ (Briggs & Beck, 2007; Manshour et al., 2016).

To evaluate the distribution $f(\mu)$, the IOTs obtained from each data set were collected in a large number of windows W_μ wider than 48 h and $\mu = \sigma_\tau^{-1}$ was measured in each window (Rabassa & Beck, 2015; Van der Straeten & Beck, 2009). Their distribution was evaluated for both the original and shuffled data sets. Figure 10 (left and middle) shows the distribution of $f(\mu)$ obtained for different W_μ and different Q. The thresholds Q have been selected in order to compare different sites possessing the same value of σ_τ. The good agreement with the theoretical χ^2 distribution is clearly observable. The number of degrees of freedom k can be related to the exponent q of equation (3) with the relation $q_{th} = 1 + 2/(k + 2)$ (Beck, 2010; Briggs & Beck, 2007; Kosun & Ozdemir, 2016). For MLO at $Q = 1$, $q = 1.67 \pm 0.10$, and $k = 2.797 \pm 0.40$, using the relation, $q_{th} = 1.4 \pm 0.4$ was obtained that, within the error bars, is in good agreement with the experimental estimation (for CVO $Q = 1$, $q = 1.690 \pm 0.07$ and $k = 2.7 \pm 0.5$ giving $q_{th} = 1.42 \pm 0.50$; for VRS $Q = 1.5$, $q = 1.582 \pm 0.1$, $k = 2.823 \pm 0.5$, and $q_{th} = 1.41 \pm 0.5$ was obtained; and for MH $Q = 1.5$, $q = 1.61 \pm 0.2$, $k = 2.88 \pm 0.2$, and $q_{th} = 1.41 \pm 0.2$).

Figure 10 (right) shows the distribution $f(\mu)$ for the shuffled data set. In this case the distribution collapses onto the same narrow distribution, completely differently from the other cases, and independent of the
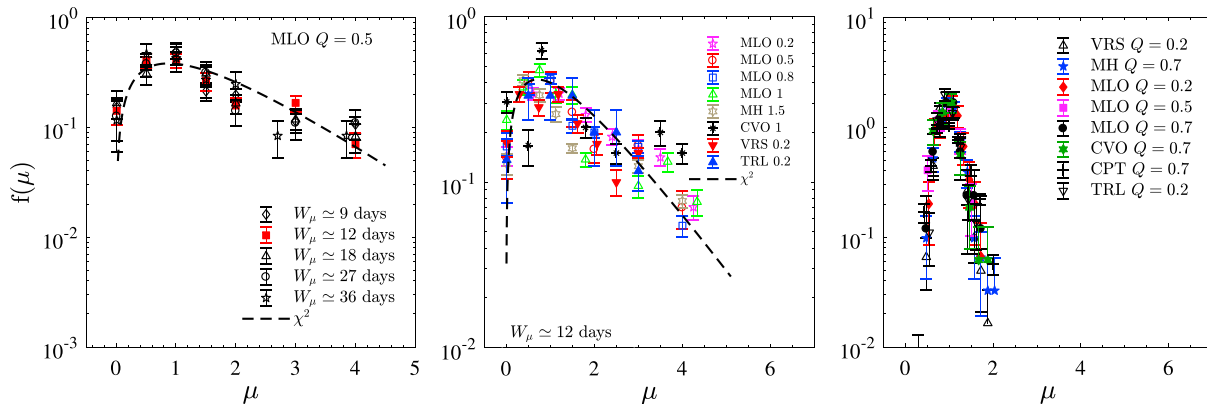
Figure 10. (left) The probability density $f(\mu)$ for the normalized IOT sequences obtained for different window sizes W_μ at a fixed threshold Q, dashed line χ^2 distribution with $k \approx 3°$ of freedom. (middle) Distribution $f(\mu)$ for different sites and different thresholds Q obtained for a window length, $W_\mu = 12$ days. The dashed line represents a theoretical χ^2 distribution with $k = 3°$ of freedom. (right) The probability density $f(\mu)$ for shuffled data for different sites and different thresholds Q.

threshold Q. This profile is in good agreement with the theoretical assumption of a delta function; however, the low data sampling rate and gaps in the data set can affect this shape and introduce a small broadening of the peak.

4. Conclusions

Through an extensive analysis of Hg^0 concentration data, measured at different latitudes and in different climatological regions, the universal behavior of the IOT extremes has been identified. The Hg^0 dynamic is characterized by a long-term memory (power law) autocorrelation function, and above a fixed threshold Q the PDFs of the IOT are described by the Tsallis q-exponential function. The PDF behavior can be explained in terms of the superstatistical nature of the IOTs, where the competition between multiple mesoscopic processes affects the macroscopic dynamics. Additionally, it seems possible that atmospheric turbulence plays a central role in the dynamics of extreme Hg^0 concentration events, since the average $\langle q \rangle = 1.59$ is comparable with the value obtained in fully developed turbulence experiments. The small differences seen in the q values obtained from the q-exponential function may be attributable to differences in the evolution of the Hg^0 concentration at each site, which would depend on the specific mesoscopic processes that occur locally and their interactions. All processes occurring in atmosphere (e.g., emission, scavenging, chemical reactions, etc.) act as a perturbation on the macroscopic dynamics of the predominant phenomenon, in this case, atmospheric transport. The extensive parameter μ encompassing all the possible fluctuations related to the mesoscopic phenomena follows a χ^2 distribution, which is effectively a "fingerprint," identifying the superstatistical nature of the overall process. By destroying the long-term memory in the data (by shuffling), the PDFs become independent from the threshold Q and the distributions all collapse on to an exponential distribution $P(\tau/\sigma_Q) = \sigma^{-1}\exp[-\tau/\sigma^{-1}]$ exposing the uncorrelated nature of the shuffled data. However, it is worth mentioning that the q values may change slightly depending on the data resolution.

References

Abe, S., & Okamoto, Y. (Eds.) (2001). *Nonextensive statistical mechanics and its applications*. Berlin Heidelberg: Springer-Verlag.

Alder, B. J., & Wainwright, T. E. (1970). Decay of the velocity autocorrelation function. *Physical Review A*, *1*, 18–21. https://doi.org/10.1103/PhysRevA.1.18

Beck, C. (2010). Generalized statistical mechanics for superstatistical systems. *Philosophical Transactions of the Royal Society of London A: Mathematical, Physical and Engineering Sciences*, *369*(1935), 453–465.

Beck, C., & Cohen, E. (2003). Superstatistics. *Physica A: Statistical mechanics and its applications*, *322*, 267–275.

Beck, C., Cohen, E. G. D., & Swinney, H. L. (2005). From time series to superstatistics. *Physical Review E*, *72*, 56133. https://doi.org/10.1103/PhysRevE.72.056133

Bogachev, M. I., & Bunde, A. (2008). Memory effects in the statistics of interoccurrence times between large returns in financial records. *Physical Review E*, *78*, 36114.

Bogachev, M. I., Eichner, J. F., & Bunde, A. (2007). Effect of nonlinear correlations on the statistics of return intervals in multifractal data sets. *Physical Review Letters*, *99*, 240601.

Briggs, K., & Beck, C. (2007). Modelling train delays with q-exponential functions. *Physica A: Statistical Mechanics and its Applications*, *378*(2), 498–504.

Bunde, A., Eichner, J. F., Kantelhardt, J. W., & Havlin, S. (2005). Long-term memory: A natural mechanism for the clustering of extreme events and anomalous residual times in climate records. *Physical Review Letters*, *94*, 48701.

Carbone, F., & Sorriso-Valvo, L. (2014). Experimental analysis of intermittency in electrohydrodynamic instability. *The European Physical Journal E*, *37*, 1–11.

Carbone, F., Gencarelli, C. N., & Hedgecock, I. M. (2016). Lagrangian statistics of mesoscale turbulence in a natural environment: The Agulhas return current. *Physical Review E*, *94*, 63101.

Carbone, F., Landis, M. S., Gencarelli, C. N., Naccarato, A., Sprovieri, F., De Simone, F., ... Pirrone, N. (2016). Sea surface temperature variation linked to elemental mercury concentrations measured on Mauna Loa. *Geophysical Research Letters*, *43*, 7751–7757. https://doi.org/10.1002/2016GL069252

Celani, A., Cencini, M., Mazzino, A., & Vergassola, M. (2004). Active and passive fields face to face. *New Journal of Physics*, *6*(1), 72.

Chelani, A. (2016). Long-memory property in air pollutant concentrations. *Atmospheric Research*, *171*, 1–4.

De Simone, F., Cinnirella, S., Gencarelli, C. N., Yang, X., Hedgecock, I. M., & Pirrone, N. (2015). Model study of global mercury deposition from biomass burning. *Environmental Science and Technology*, *49*(11), 6712–6721.

De Simone, F., Artaxo, P., Bencardino, M., Cinnirella, S., Carbone, F., ... Pirrone, N. (2017). Particulate-phase mercury emissions from biomass burning and impact on resulting deposition: A modelling assessment. *Atmospheric Chemistry and Physics*, *17*(3), 1881–1899.

Douglas, P., Bergamini, S., & Renzoni, F. (2006). Tunable Tsallis distributions in dissipative optical lattices. *Physical Review Letters*, *96*, 110601. https://doi.org/10.1103/PhysRevLett.96.110601

Dvonch, J. T., Keeler, G. J., & Marsik, F. J. (2005). The influence of meteorological conditions on the wet deposition of mercury in southern Florida. *Journal of Applied Meteorology*, *44*(9), 1421–1435.

Eichner, J. F., Kantelhardt, J. W., Bunde, A., & Havlin, S. (2007). Statistics of return intervals in long-term correlated records. *Physical Review E*, *75*, 11128.

Ferri, G., Savio, M. R., & Plastino, A. (2010). Tsallis' triplet and the ozone layer. *Physica A: Statistical Mechanics and its Applications*, *389*(9), 1829–1833.

Ferri, G. L., Figliola, A., & Rosso, O. A. (2012). Tsallis' statistics in the variability of El Niño/Southern Oscillation during the Holocene epoch. *Physica A: Statistical Mechanics and its Applications*, *391*(5), 2154–2162.

Frisch, U. (Ed.) (1995). *Turbulence: The legacy of A. N. Kolmogorov*. Cambridge UK: Cambridge University Press.

Hayley, H. S., Alexander, H. D. C., Keh-Han, W., Michelle, H. T., & Clark, C. K. L. (Eds.) (2002). *Environmental fluid mechanics: Theories and applications*. Reston, VA: American Society of Civil Engineer.

Holmes, C. D., Krishnamurthy, N. P., Caffrey, J. M., Landing, W. M., Edgerton, E. S., Knapp, K. R., & Nair, U. S. (2016). Thunderstorms increase mercury wet deposition. *Environmental Science & Technology*, *50*(17), 9343–9350.

Horowitz, H. M., Jacob, D. J., Zhang, Y., Dibble, T. S., Slemr, F., Amos, H. M., . . . Sunderland, E. M. (2017). A new mechanism for atmospheric mercury redox chemistry: Implications for the global mercury budget. *Atmospheric Chemistry and Physics Discussions*, *17*, 6353–6371.

Istas, J., & Lang, G. (1997). Quadratic variations and estimation of the local Hölder index of a Gaussian process. *Annales de l'Institut Henri Poincare (B) Probability and Statistics*, *33*(4), 407–436.

Katul, G., Porporato, A., Cava, D., & Siqueira, M. (2006). An analysis of intermittency, scaling, and surface renewal in atmospheric surface layer turbulence. *Physica D: Nonlinear Phenomena*, *215*(2), 117–126.

Kosun, C., & Ozdemir, S. (2016). A superstatistical model of vehicular traffic flow. *Physica A: Statistical Mechanics and its Applications*, *444*(Supplement C), 466–475.

Landis, M. S., Stevens, R. K., Schaedlich, F., & Prestbo, E. M. (2002). Development and characterization of an annular denuder methodology for the measurement of divalent inorganic reactive gaseous mercury in ambient air. *Environmental Science & Technology*, *36*(13), 3000–3009.

Landis, M. S., Vedantham, R., & Alvarez-Aviles, L. (2013). Measurements of ambient mercury and related species at the Mauna Loa observatory 2002–2010. In *11th International Conference of Mercury as a Global Pollutant*. Edinburgh, Scotland. Retrieved from https://www.esrl.noaa.gov/gmd/publications/annual_meetings/2010/pdfs/3-Krnavek.pdf

Lindberg, S. E., Brooks, S., Lin, C.-J., Scott, K. J., Landis, M. S., Stevens, R. K., . . . Richter, A. (2002). Dynamic oxidation of gaseous mercury in the arctic troposphere at polar sunrise. *Environmental Science & Technology*, *36*(6), 1245–1256.

Lovejoy, S., & Schertzer, D. (2013). *The weather and climate: Emergent laws and multifractal cascades*. Cambridge: Cambridge University Press.

Manshour, P., Anvari, M., Reinke, N., Sahimi, M., & Tabar, M. R. R. (2016). Interoccurrence time statistics in fully-developed turbulence. *Scientific Reports*, *6*, 27452.

Mazzitelli, I., & Lanotte, A. S. (2012). Active and passive scalar intermittent statistics in turbulent atmospheric convection. *Physica D: Nonlinear Phenomena*, *241*(3), 251–259. https://doi.org/10.1016/j.physd.2011.07.009

McComb, W. D. (Ed.) (1990). *The physics of fluid turbulence*. New York: Oxford University Press.

Monin, A. S., & Yaglom, A. M. (Eds.) (2007). *Statistical fluid mechanics: Mechanics of turbulence*. New York: Dover.

Pirrone, N., Cinnirella, S., Feng, X., Finkelman, R. B., Friedli, H. R., Leaner, J., . . . Telmer, K. (2010). Global mercury emissions to the atmosphere from anthropogenic and natural sources. *Atmospheric Chemistry and Physics*, *10*(13), 5951–5964.

Rabassa, P., & Beck, C. (2015). Superstatistical analysis of sea-level fluctuations. *Physica A: Statistical Mechanics and its Applications*, *417*, 18–28.

Ryan, S. (1997). The wind field around Mauna Loa derived from surface and balloon observations. *Journal of Geophysical Research*, *102*(D9), 10,711–10,725.

Santhanam, M., & Kantz, H. (2005). Long-range correlations and rare events in boundary layer wind fields. *Physica A: Statistical Mechanics and its Applications*, *345*(3–4), 713–721. https://doi.org/10.1016/j.physa.2004.07.012

Schertzer, D., & Lovejoy, S. (1985). *The dimension and intermittency of atmospheric dynamics* (pp. 7–33). Berlin, Heidelberg: Springer Berlin Heidelberg.

Schertzer, D., & Lovejoy, S. (1987). Physical modeling and analysis of rain and clouds by anisotropic scaling multiplicative processes. *Journal of Geophysical Research*, *92*(D8), 9693–9714. https://doi.org/10.1029/JD092iD08p09693

Schroeder, W. H., & Munthe, J. (1998). Atmospheric mercury — An overview. *Atmospheric Environment*, *32*(5), 809–822.

Schroeder, W. H., Anlauf, K. G., Barrie, L. A., Lu, J. Y., Steffen, A., Schneeberger, D. R., & Berg, T. (1998). Arctic springtime depletion of mercury. *Nature*, *394*(6691), 331–332. https://doi.org/10.1038/28530

Sharma, N. C., & Barnes, J. E. (2016). Boundary layer characteristics over a high altitude station, Mauna Loa Observatory. *Aerosol and Air Quality Research*, *16*(3), 729–737.

Sprovieri, F., Pirrone, N., Bencardino, M., D'Amore, F., Carbone, F., Cinnirella, S., . . . Norstrom, C. (2016). Atmospheric mercury concentrations observed at ground-based monitoring sites globally distributed in the framework of the GMOS network. *Atmospheric Chemistry and Physics*, *16*(18), 11,915–11,935. https://doi.org/10.5194/acp-16-11915-2016

Steffen, A., Douglas, T., Amyot, M., Ariya, P., Aspmo, K., Berg, T., . . . Temme, C. (2008). A synthesis of atmospheric mercury depletion event chemistry in the atmosphere and snow. *Atmospheric Chemistry and Physics*, *8*(6), 1445–1482. https://doi.org/10.5194/acp-8-1445-2008

Steffen, A., Lehnherr, I., Cole, A., Ariya, P., Dastoor, A., Durnford, D., . . . Pilote, M. (2015). Atmospheric mercury in the Canadian Arctic. Part I: A review of recent field measurements. *Science of The Total Environment*, *509–510*, 3–15. Special Issue: Mercury in Canada's North.

Tsallis, C. (1988). Possible generalization of Boltzmann-Gibbs statistics. *Journal of Statistical Physics*, *52*(1), 479–487.

Tsallis, C., & Souza, A. M. C. (2003). Constructing a statistical mechanics for Beck-Cohen superstatistics. *Physical Review E*, *67*(2), 26106. https://doi.org/10.1103/PhysRevE.67.026106

Tsallis, C., Mendes, R., & Plastino, A. (1998). The role of constraints within generalized nonextensive statistics. *Physica A: Statistical Mechanics and its Applications*, *261*(3–4), 534–554.

Tuck, A. F. (2010). From molecules to meteorology via turbulent scale invariance. *Quarterly Journal of the Royal Meteorological Society*, *136*(650), 1125–1144.

Van der Straeten, E., & Beck, C. (2009). Superstatistical fluctuations in time series: Applications to share-price dynamics and turbulence. *Physical Review E*, *80*, 36108. https://doi.org/10.1103/PhysRevE.80.036108

van Kampen, N. (Ed.) (1981). *Stochastic processes in physics and chemistry*. Amsterdam: North-Holland.

Vindel, J. M., & Yagüe, C. (2011). Intermittency of turbulence in the atmospheric boundary layer: Scaling exponents and stratification influence. *Boundary-Layer Meteorology*, *140*(1), 73–85.

Warhaft, Z. (2000). Passive scalars in turbulent flows. *Annual Review of Fluid Mechanics*, *32*(1), 203–240.

Wilk, G., & Włodarczyk, Z. (2000). Interpretation of the nonextensivity parameter q in some applications of Tsallis statistics and Levy distributions. *Physical Review Letters*, *84*, 2770–2773. https://doi.org/10.1103/PhysRevLett. 84.2770

Wyngaard, J. C. (1992). Atmospheric turbulence. *Annual Review of Fluid Mechanics*, *24*, 205.